Available online at www.sciencedirect.com
ScienceDirect
Polymer 48 (2007) 7176–7192
polymer
www.elsevier.com/locate/polymer

Dynamic phase diagram derived from large deformation non-linear mechano-optical behavior of polyethylene naphthalate nanocomposites

K. Kanuga, M. Cakmak*

Polymer Engineering Department, University of Akron, Akron, OH 44325-0301, United States

Received 15 August 2007; received in revised form 19 September 2007; accepted 24 September 2007
Available online 5 October 2007

Abstract

The effect of nanoparticles on the mechano-optical behavior of PEN was investigated using a real time true stress–true strain birefringence measuring system [Toki S, Valladares D, Sen TZ, Cakmak M. ANTEC Proc 2001:1830; Koike Y, Cakmak M. Polymer 2003;44:4249]. The large deformation stress–optical behavior revealed that there are at most three distinct regimes that may be augmented by an initial additional glassy component at lower temperatures and/or high rates. The presence of nanoparticles did not change the birefringence development of PEN before strain induced crystallization. However, after strain induced crystallization occurred in PEN, the birefringence increase was found to be diminished due primarily to the decrease in the amount of crystallinity and amorphous chain orientation with the addition of nanoparticles. The final structure and deformation behavior of the nanocomposites have been mapped out in a dynamic phase diagram as a function of stretching temperature, rate and nanoparticle content. This dynamic phase diagram shows that the material undergoes three critical structural transitions: (i) nematic–crystalline transition wherein the material stretched below a certain temperature does not undergo orientation-induced crystallization but develops a highly ordered nematic state. (ii) A kinematic transition wherein the material transforms from a 'structured liquid' to a 'true liquid' state exhibited by the disappearance of the initial glassy component as the material becomes devoid of the inherent structure due to segmental correlations. (iii) While unfilled PEN remains amorphous at high temperatures due to high relaxation rates combined with decreased thermal crystallizability, the presence of nanoplatelets was found to facilitate strain induced crystallization even at such high temperatures primarily due to the decrease in orientation relaxation in their presence.

Keywords: Mechano-optical; Stress–optical; Birefringence

1. Introduction

PEN (polyethylene naphthalate) is a slow crystallizing polymer with a moderately high glass transition temperature around 120 °C due to the presence of naphthalene groups along its chain. This polymer, like its close chemical relative, PET, can be quenched into an amorphous state and can also be crystallized either by slow cooling from the melt or by stretching between the glass transition temperature and the cold crystallization temperature [3].

One of the unusual characteristics of PEN is that it shows necking upon stretching from the amorphous state above the glass transition temperature. This was shown to be caused by the highly cooperative orientation of naphthalene planes parallel to the surface of the film [3]. This results in uneven thickness distribution that is detrimental to the appearance and the final properties of the product. Blending of polyetherimide (PEI) with PEN has been shown to eradicate necking by hindering the alignment of the naphthalene rings [4]. Although the addition of PEI into PEN eliminates necking it has its own disadvantages. PEI being an amorphous material decreases the crystallizability of PEN rendering the material completely amorphous beyond 20% PEI content in the blend. This absence of crystallinity in the material is detrimental to the processability and final product properties specifically tensile strength and dimensional stability of the material. Hence a solution to necking in PEN is desired which not only eliminates necking but also avoids significant decrease in crystallizability of the material.

* Corresponding author.
E-mail address: cakmak1@uakron.edu (M. Cakmak).

0032-3861/$ - see front matter © 2007 Elsevier Ltd. All rights reserved.
doi:10.1016/j.polymer.2007.09.047

Recently, nanocomposites have received academic as well as industrial research focus. Front-runner in this field is montmorillonite (MMT) clay based polymer nanocomposites. Molecular dispersion of these MMT nanoparticles has led to a drastic increase in barrier properties, mechanical properties like modulus to a lesser extent tensile strength, thermal properties like melting point and HDT [5–8]. These montmorillonite nanoparticles have a specific platelet structure in the form of layered sheets with tetrahedral shaped anionic (SiO_4) groups and the thickness of each layered sheet is around 10 Å with a high aspect ratio of 400–800:1 [9] which is an important factor in understanding the drastic increase in the properties described above. Dispersion of these relatively stiff nanoparticles in the PEN matrix could help to introduce more inter-chain friction in-between the naphthalene groups that, in turn, help pre-orient the naphthalene groups cooperatively parallel to the surface of the film during melt casting process hence preventing necking during the rubbery state deformation typical of film processing operations. PEN and its nanocomposites hence have the potential to be widely used in film and bottling applications due to its high glass transition temperature, high barrier coupled with better dimensional stability. All these product manufacturing processes will require deformation of the polymer above its glass transition temperature causing significant polymer orientation, crystallization and a sequence of structural ordering processes that ultimately determine the physical properties of the product. Moreover, polymer orientation and crystallization processes are controlled by the stretching temperature and deformation rate. Hence it is critical to study the effect of processing conditions on the structural organization processes that take place during deformation to control the properties of the final product. Birefringence measurement is a robust quantitative technique that gives insight into the mechanistic changes taking place during deformation as well as polymer orientation when captured real time. Moreover birefringence measurements when coupled with true mechanical behavior measurements and off-line characterization studies provide a deeper and a complete insight into temporal evolution of mechanistic changes taking place during deformation [10,11]. Studies on the structural details using birefringence have been reported wherein the birefringence–stress behavior during deformation in the rubbery state has been investigated in PET [12], PEN [13] and some amorphous polymers such as PS and PC [14].

This research is focused on investigating the effect of nanoparticles on necking behavior in PEN in rubbery state deformation from amorphous precursors. This study also includes the effect of these nanoparticles on the mechano-optical behavior, crystallization as well structure ordering processes taking place during uniaxial deformation. This helps in developing detailed map of the effect of nanoparticle addition, stretching temperature and deformation rate on the material phase behavior. A recently developed stretching system [1,2] that acquires birefringence simultaneously with true mechanical behavior of the material as it is being stretched will be used to determine the mechanistic changes as reflected in mechano-optical behavior of the films. The key structural changes responsible for the latter mechanistic changes will be elucidated with the off-line structural characterization techniques.

2. Experimental

2.1. Materials

Melt cast amorphous PEN 100 μm thick sheets containing organically modified clay concentrations ranging 0.5–2 wt% was kindly provided by Teijin Chemical Co. Along with the nanocomposites unfilled PEN was used as a control. All samples were found to be transparent.

2.2. Online birefringence and true mechanical behavior measurements

A special instrumented stretching machine [1,2] was used to simultaneously determine the mechanical and optical properties of polymer films during uniaxial deformation. The design of this machine includes three parts: the uniaxial stretching system with two moving crossheads allows the mid symmetry of the sample to remain stationary during stretching. The sample is surrounded by an air circulating environmental chamber with external heater system. With the designed-in optical flats on front and back walls of the chamber, the spectral birefringence and sample width (with a laser micrometer) are continuously monitored during and after the stretching. Real time measurements of optical retardation, sample width, force and elongation are recorded simultaneously. Assuming (1) simple extension and (2) incompressibility, time variation of the local thickness is calculated and thus birefringence, local true stress and local true strain are determined.

Change in volume due to the development of crystallinity in the material would be expected to occur. But as will be shown in this paper the degree of crystallinity developed in the samples ranges anywhere from 0% to 30%. The volume change between these states is approximately 2.5% ($\rho_c = 1.407$ g/cm [3,15], $\rho_a = 1.325$ g/cm [3,16]). Since the development of crystallinity occurs towards the end of high strain stretching, the error committed by this incompressibility assumption is negligible during substantial part of the deformation and maximum error – though quite low – occurs at the end of large deformation stage. In addition, assuming any changes in volume would affect all dimensions equally and the width being measured real time reduces the committed error. We have verified this assumption with off-line thickness measurements taken for different deformation levels as well as different stretching conditions and compared them with on-line thickness values obtained from width measurements. These data are shown in Fig. 1 where good correlation is observed between them. Additional details of the system can be found elsewhere [1,2]. The birefringence measurements taken in this study are reported for the wavelength of 546 nm.

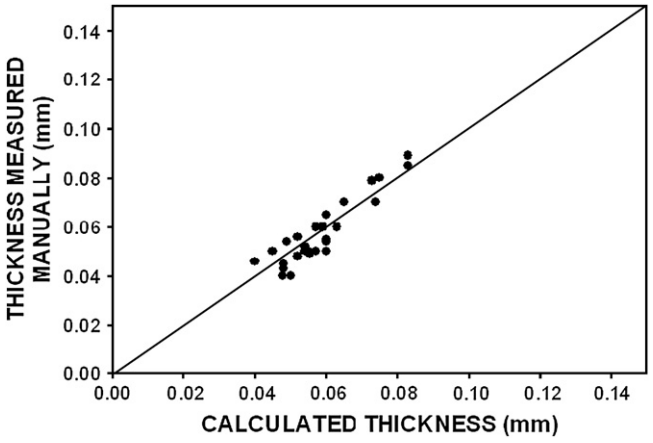

Fig. 1. Calculated online (using incompressibility assumption) vs off-line manual thickness measurements (using precision micrometer).

2.3. Sample preparation

Dumbbell-shaped specimens were cut from the original melt cast and amorphous films with the following dimensions: 75 mm long, 40 mm wide and 30 mm wide in the narrowest region as shown in the figure below (Fig. 2). The samples were clamped and fixed in the arms of the uniaxial stretching system inside the environmental oven. The distance between the clamps was taken as 30 mm.

2.4. Thermal characterization

Thermal properties of PEN and its nanocomposites were measured using a universal 2920 MDSC V2.6A TA Instruments DSC. The samples of approximately 6–10 mg were crimped in aluminum pans and were scanned at a heating rate of 20 °C/min under a dry nitrogen blanket. The reported transition temperatures (T_{cc}, T_m) are referring to the peak maximum position and T_g is referred as the midpoint of the glass transition. The degree of crystallinity of the PEN was determined using the equation below and was normalized to the fraction of PEN present in the mixture:

$$\text{Crystallinity}\ (\%) = \left(\Delta H_{exp}/\Delta H^{o}\right) \times 100$$

where $\Delta H_{exp} = \Delta H_{melting} - \Delta H_{cold\ \ crystallization}$ and ΔH^{o} (103.4 J/g [17]) is the heat of fusion for 100% crystalline PEN.

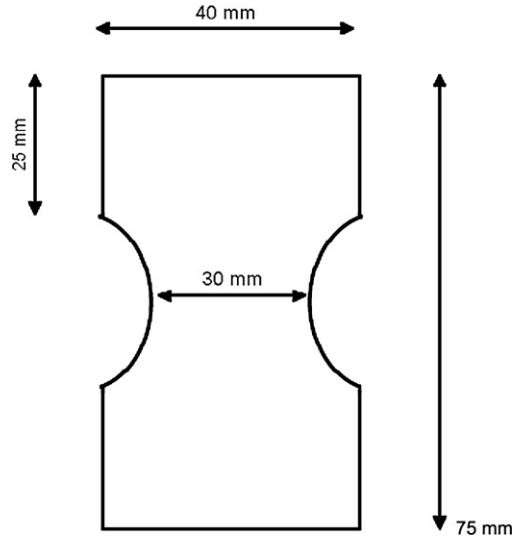

Fig. 2. Sample dimensions.

2.5. WAXD measurements

Bruker AXS Generator equipped with a copper target tube and a two dimensional detector was used to obtain the one-quadrant of the WAXD patterns of the stretched samples. Monochromatized Cu Kα radiation was obtained by operating the generator at 40 kV and 40 mA. A typical exposure time of 20 min was used.

The crystal size was measured by applying Scherrer equation to the data obtained by the Bruker X-ray machine. The data collected are then used to calculate half width of the (010) peak as well as the maximum scattering angle. The equation is given as:

$$L_{hkl} = \frac{K\lambda}{\beta_0 \cos\theta}$$

where L_{hkl} is the mean dimension of the crystallites perpendicular to the planes (hkl), β_0 is the integral breadth or breadth at half maximum intensity of the pure reflection profile in radians and K is a constant that is commonly assigned a value of unity.

To determine the crystalline orientation factor for the chain axis, we have defined a pseudo-orthorhombic unit cell for the PEN single chain. The details regarding the axis of the new unit cell as well as the angles between the axis of the pseudo-orthorhombic cell and the poles of the selected planes of the original triclinic unit cell are given in an earlier paper [18].

From Wilchinsky's rule the $\cos^2\chi$ values of the chain (C-axis) become:

$$\cos^2\chi_{(c,z)} = 1 - 0.844\cos^2\chi_{(\bar{1}10,z)} - 1.156\cos^2\chi_{(010,z)}$$

Finally the orientation factor is given by:

$$f_c = \frac{\left(3\langle\cos^2\chi_{c,z}\rangle - 1\right)}{2}$$

The amorphous chain orientation factor is calculated using the crystalline orientation factor, intrinsic birefringence values of the amorphous as well as crystalline material and the total birefringence of the stretched sample as described below.

$$\Delta n = f_a\Delta n_a(1 - x_c) + f_c\Delta n_c x_c$$

The birefringence as well as form birefringence contribution of the nanoparticles was considered negligible as we are passing the light through the normal direction of the film. In this condition the in-plane intrinsic birefringence of the nanoparticles is almost zero [19] as their orientation in the film plane is random and the average will contribute isotropically to the incoming light. There is no form birefringence contribution

from the nanoparticles as the light is passed normal to the film plane and it is traveling normal to the plane of the nanoparticles. Stretching the polymer films would cause some orientation of the nanoparticles. However, the intrinsic birefringence of the clay nanoparticles being two magnitudes lower (0.019–0.065 [19]) than the intrinsic birefringence of PEN (= 0.75 [20]) and the concentration of the nanoparticles reaching its highest levels of 2 wt% in PEN, the contribution of nanoparticles to the birefringence of PEN is negligible.

3. Results and discussion

3.1. Thermal properties of as-cast films

As-prepared melt cast samples are essentially amorphous as shown in Fig. 3, where DSC thermograms for PEN-controlled, PEN–Nano-0.5%, PEN–Nano-1% and PEN–Nano-2% nanocomposites are presented. A slight increase in the midpoint of the T_g is observed with the addition of clay particles.

Both the breadth of T_g ($T_{g\ start} - T_{g\ end}$) and the delta T_g (half width at the half height of the first derivative) [Fig. 4] indicate that there is a broadening of the glass transition with increasing nanoparticle concentration indicating the presence of heterogeneities in the material as the nanoparticle content is increased. Moreover the increasing breadth of T_g towards higher temperatures also indicates that there is growing number of chains in the material with decreased mobility presumably those chains which are entrapped between the nanoparticles or in their proximity.

The cold crystallization temperature with the addition of nanoparticles finally drops down to 198 °C for PEN–Nano-2%. The decrease in the T_{cc} with increasing nanoparticle content shows that the nanoparticles play a role of cold crystallization nucleating agent during heating from the amorphous state. The melting temperature essentially remains at 266 °C and does not change with the addition of nanoparticles.

3.2. Dynamic mechanical analysis

Fig. 5 shows the tan δ vs temperature plots for PEN as well as PEN nanocomposites with nanoparticle concentration ranging from 0.5 wt% to 2 wt%. Two relaxation processes are observed below the glass transition as indicated by the peaks in the tan δ. They are known as β (carbonyl group motion) and β* (naphthalene group motion) in the order of increasing temperature [21]. Increasing the nanoparticle concentration decreases the area under the peaks of both the relaxation processes indicating diminished motion of the carbonyl as well naphthalene groups in the PEN chain.

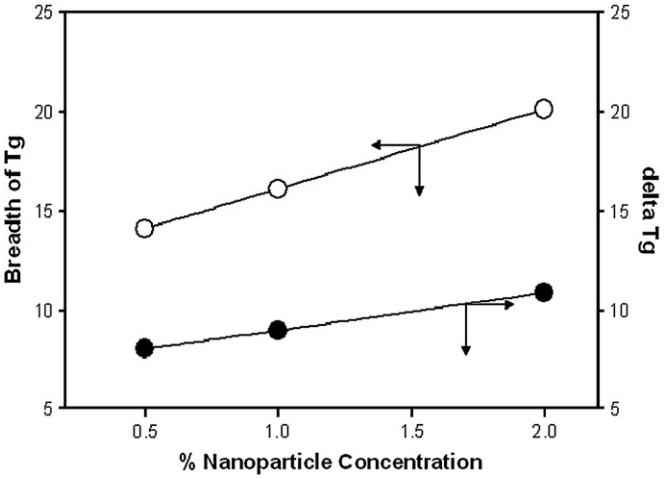

Fig. 4. Breadth of T_g and delta T_g as a function of nanoparticle concentration.

3.3. State of dispersion of the nanoparticles in PEN

Exfoliation and general dispersion of nanoparticles in PEN are investigated using TEM and WAXD as well as wide angle X-ray pole figure analysis as shown in Figs. 6 and 7. It is clear from the TEM images that no significant aggregation is visible. The clay nanoparticles are dispersed in the PEN matrix in the form of stacks ranging from 3 nm to 9 nm in thickness. This implies that the observed layers are composed of multiple elementary layers stacked on top of each other. Increasing the clay loading from 0.5% to 2% does not show any significant changes in the dispersion of the clay particles in the polymer.

X-ray analyses have shown that the structure is intercalated with a *d*-spacing of approximately 25 Å. Wide angle X-ray

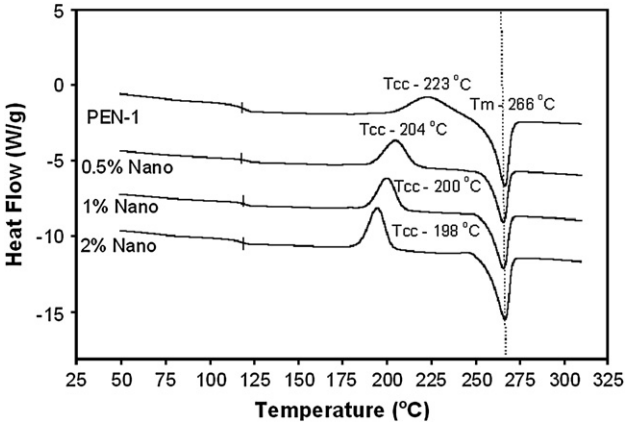

Fig. 3. DSC thermograms of melt cast films.

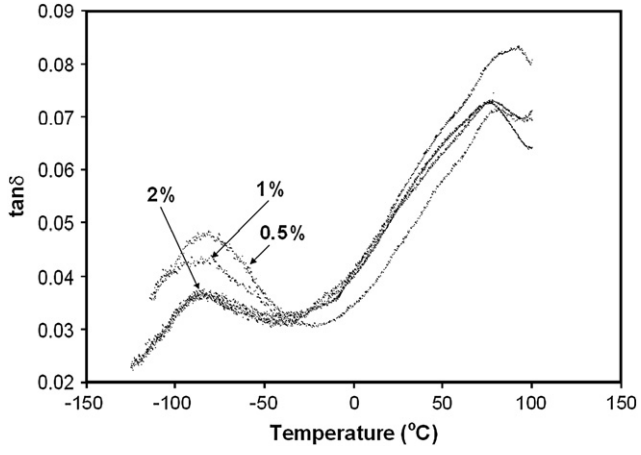

Fig. 5. DMA analysis of PEN nanocomposites at 1 Hz frequency.

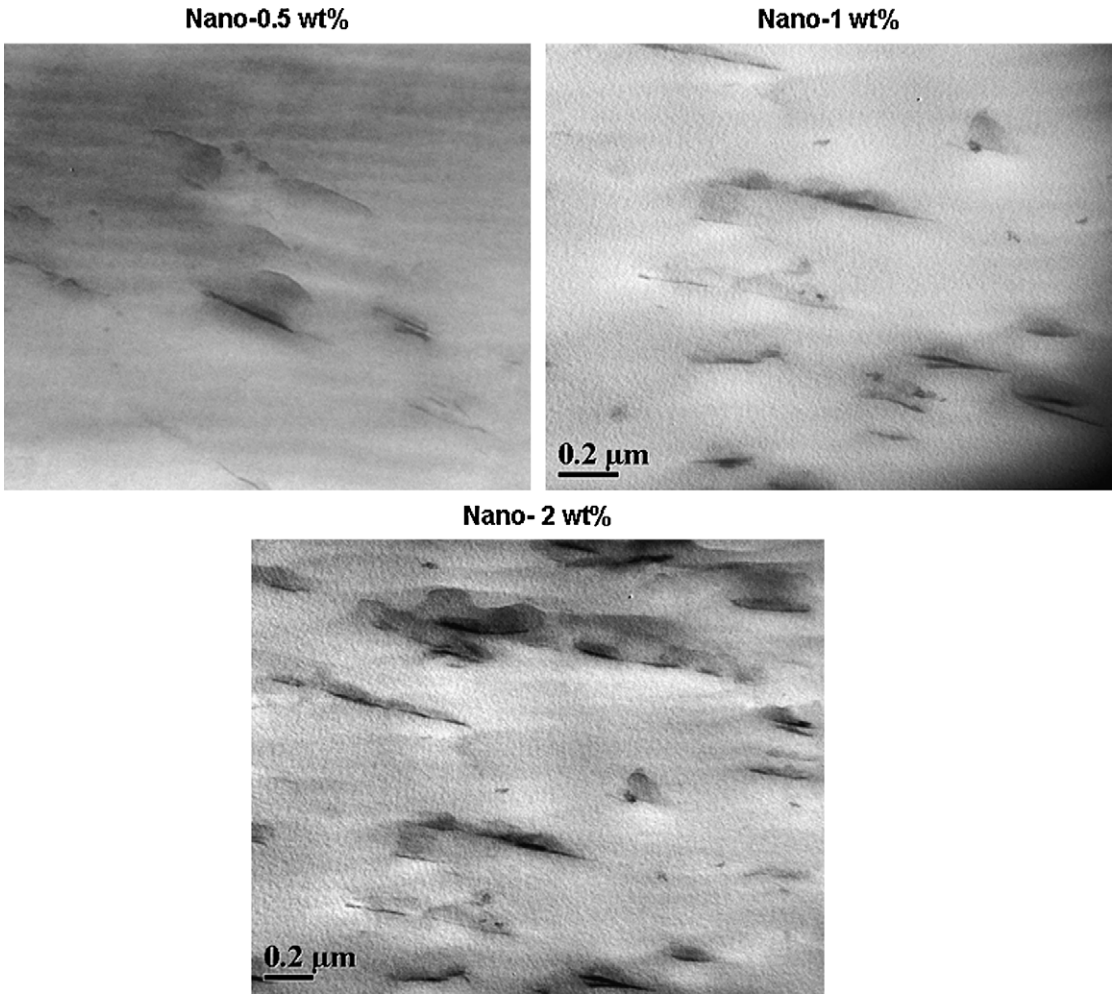

Fig. 6. TEM images of PEN nanocomposite with different nanoparticle concentrations.

diffraction patterns taken in the transmission mode for 0.5 wt% and 1 wt% nanomaterials do not display any peak at the low angles of interest. This is a result of development of preferred orientation of the nanoparticles with their broad surfaces parallel to the film plane during the casting process.

As we increase the content of nanoparticles to 2 wt% the intensity scans taken in the transmission mode show a peak

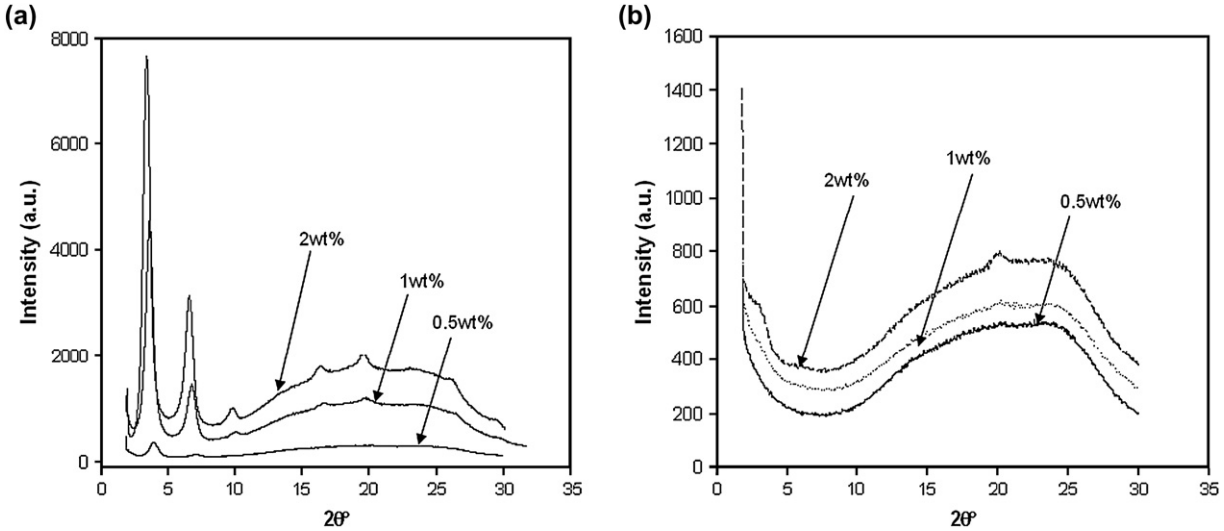

Fig. 7. (a) X-ray diffraction patterns in reflection mode; (b) X-ray diffraction patterns in transmission mode.

corresponding to the nanoparticles that indicates that some of the nanoparticles are tilted with respect to the film plane. X-ray diffraction patterns taken in the reflection mode for different nanoparticle compositions exhibit a diffraction peak near 3.4° corresponding to a main gallery spacing (d_{001}), 2.5 nm, along with other higher order peaks. This indicates significant order in the materials for all three nanoparticle compositions and the height of the peaks increases with increasing nanoparticle content due to increase in the concentration of the nanoparticles.

Combining the results from X-ray and TEM shows that there is co-occurrence of partially exfoliated and intercalated structures in the nanocomposites where the nanoplatelets are organized in stacks that are 2.5 nm apart.

The WAXD pole figure taken at 3.4° 2θ on as-cast unstretched film containing 2% nanocomposite is shown in Fig. 8. The (001) plane poles are concentrated normal to the film surface that clearly indicate that these nanoclay crystals have already attained high orientation levels with their broad surfaces (that are normal to the (001) planes) becoming parallel to the film surface during the melt casting process.

One of the unusual characteristics of PEN is that it shows necking behavior upon stretching from the amorphous state above the glass transition temperature. In one of the earlier publications [4] we have reported that this neck formation is a result of a highly localized cooperative orientation of the naphthalene planes parallel to the surface of the film. In this earlier study [4] we also noted a rapid drop in the measured stretching force accompanying the initial neck formation. This suggested that when the naphthalene planes are aligned parallel to the broad surface of the sample the inter-chain friction is greatly reduced as a result of this 'graphitic' orientation behavior of the naphthalene planes. To counteract this behavior we have undertaken this present study wherein nanoparticles are added to PEN to increase inter-chain friction and hence avoid necking. Another reason for adding nanoparticles

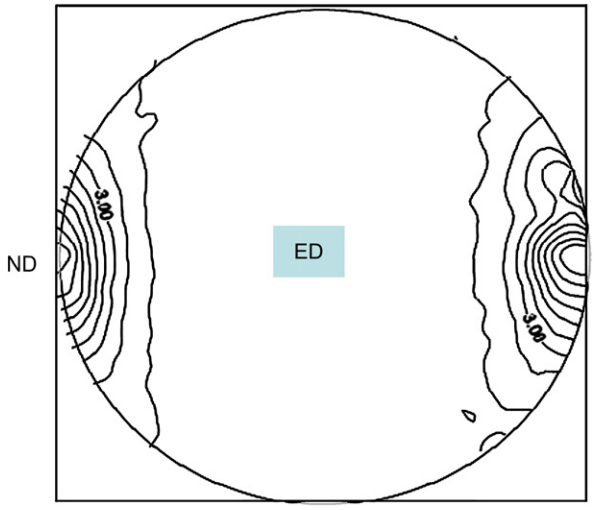

Fig. 8. Wide angle X-ray pole figure of clay (001) basal planes on cast unstretched films. (Center = extrusion direction, horizontal axis = normal (film) direction.)

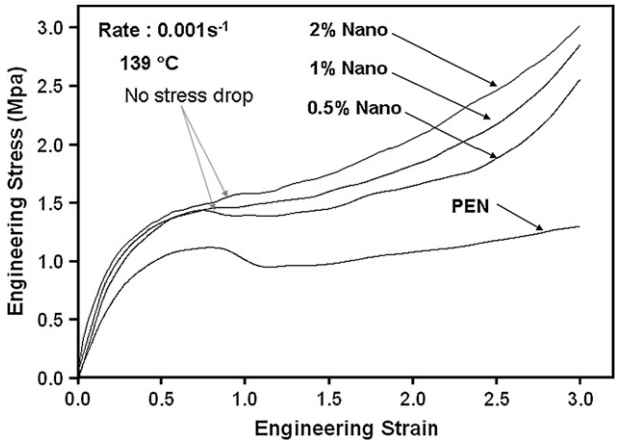

Fig. 9. Engineering stress–strain curves for PEN with different nanoparticle concentrations.

is to pre-align the naphthalene rings during the film melt casting process. Nanoparticles due to their platelet type structure would act as flat sheets to help align the naphthalene rings during film casting process and hence prevent necking during the stretching process. Fig. 9 shows the engineering stress–strain behavior of PEN nanocomposites at 139 °C and 0.001 s^{-1} stretching rate. It shows that PEN and PEN–Nano-0.5% show a stress drop during yielding which is a clear sign of necking in the materials but as we increase the nanoparticle content to 1 wt% and beyond we see no such stress drop during yielding indicating that necking is eliminated with the addition of as little as 1 wt% nanoparticles in PEN.

3.4. True mechanical behavior

True stress–true strain behavior of the PEN nanocomposites as a function of composition is shown in Fig. 10. The laser micrometer placed in the system continuously measures the width of the sample during deformation giving a true

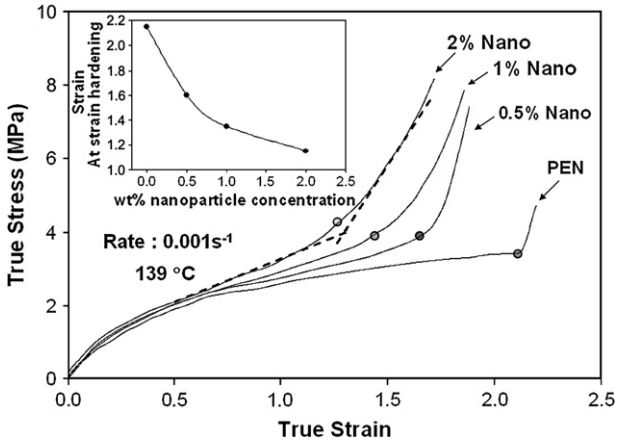

Fig. 10. Effect of nanoparticle concentration on the true stress–true strain curves at 0.001 s^{-1} and engineering stretch ratio of 4×. (The method of onset of strain hardening is schematically shown on data for 2% Nano with dashed line intersection.)

representation of the material response to deformation. As a result the start of strain hardening is easily pinpointed in such data. The addition of nanoparticles in PEN causes an early onset of strain hardening as quantitatively shown in the inset of Fig. 10. This behavior is governed by the mobility of the polymer chains during deformation and any hindrance to the movement of polymer molecules or in other words any 'rigidifying effect' in the material will cause an early onset of strain hardening and vice versa.

Addition of high aspect ratio nanoparticles shifts the T_g to higher temperature and the breadth of the T_g increases. This indicates that polymer chains in the intergallery spacing between the nanoparticles and those wrapped around the particles have decreased chain mobility showing a transition at higher temperature as discussed in the above section. This effect is also supported by the DMA analysis (Fig. 5) which shows the peak height and area under the peak of the carbonyl group as well as the naphthalene ring vibration going down with the addition of nanoparticles. In addition to this effect, there is a decline in the relaxation of the oriented polymer chains closely associated with the nanoparticles as the presence of stiff nanoparticles does not allow the polymer chains to recoil as much, as they are wrapped around or in-between the intergallery spacing of the nanoparticles. Under this condition of decreased mobility as well as relaxation, the polymer chains will reach their finite chain extensibility earlier and hence their strain hardening occurs at lower true strains. The true stress levels developed in the material also increase with increasing nanoparticle content due to the increase in stiffness of the nanocomposites as expected.

3.5. Effect of temperature on the mechano-optical behavior

The effect of stretching temperature on the mechano-optical behavior of PEN nanocomposites is shown in Figs. 11–14 for 2 wt% Nano and 0.5 wt% nanomaterials, along with the WAXD patterns taken at the end of the stretching process. In Fig. 11, we also illustrate the regime behavior for four different cases.

To investigate this effect the as-cast films of the nanocomposites are stretched above their respective glass transition temperatures when the films exist in the rubbery state. Stretching is performed at different temperatures to the same final stretch ratio while thermal crystallizability is still substantially reduced in this temperature window as illustrated in Fig. 3. As shown in Figs. 11 and 13, PEN nanocomposites exhibit a three-regime stresseoptical behavior in the temperature range of $T_g + 20$ °C to $T_g + 32$ °C (143–160 °C). Initially in Regime I the stresseoptical behavior remains linear following the generalized stresseoptical rule. On further deformation, the stress–optical behavior positively deviates from linearity and follows a steep slope with a significant increase in birefringence with little change in stresses. After Regime II, the stress–optical behavior negatively deviates into Regime III where stresses increase while birefringence reaches a plateau. The stress–optical behavior in this temperature range is characterized as Regime I–II–III behavior.

Stretching the nanocomposites in the range of $T_g + 14$ °C to $T_g + 20$ °C (134, 138 °C), the stress–optical behavior exhibits an initial glassy behavior as the deformation begins where the

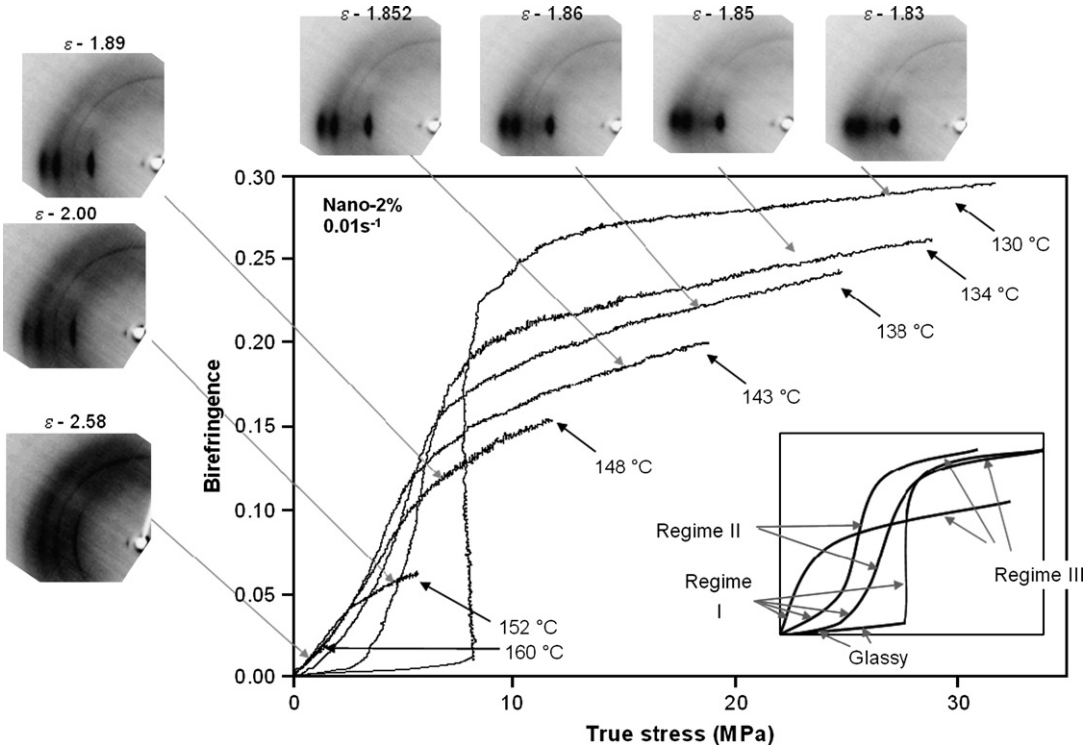

Fig. 11. Temperature effect on the stress–optical behavior of PEN with 2 wt% nanoparticles stretched at 0.01 s^{-1} engineering strain rate and final stretch ratio 4×. (Regimes for four distinct behaviors are identified in the sketch are shown in the inset.)

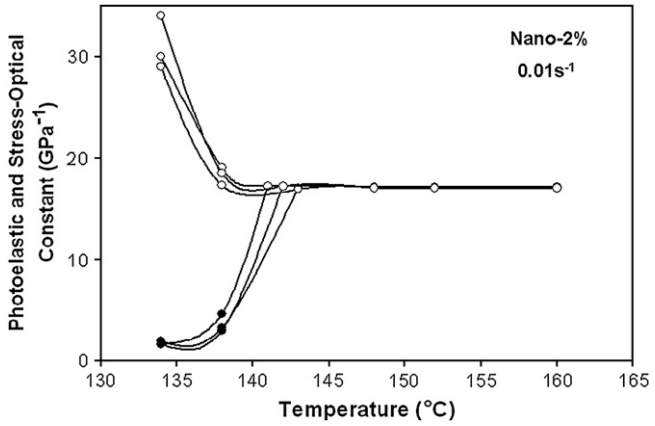

Fig. 12. Photoelastic (closed symbols) and Regime I (open symbols) slope as functions of temperature for PEN with 2 wt% nanoparticles stretched at 0.01 s^{-1} engineering strain rate and final stretch ratio 4×.

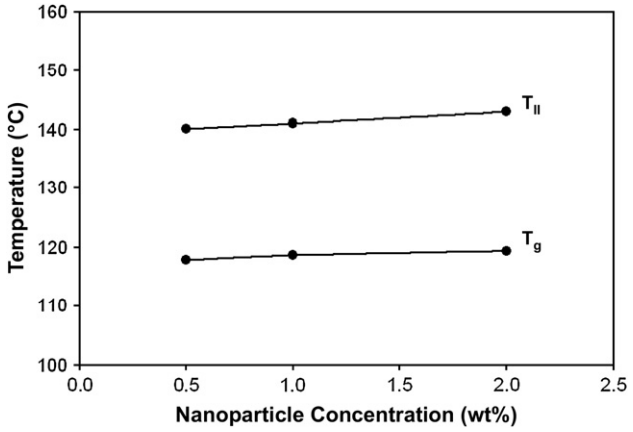

Fig. 14. T_{II} and T_g as functions of nanoparticle concentration.

stresses increase with small change in birefringence. After exhibiting this glassy behavior, further stretching the material shows rubber-like deformation behavior wherein birefringence increases linearly with stress denoted as 'Regime I'. The slope of Regime I decreases as the temperature increases. On further deformation the deviation from linearity occurs and birefringence increases steeply with stress. Following this 'Regime II' behavior birefringence starts to reach a plateau while stresses increase significantly in the final stage 'Regime III' as the chains reach their finite chain extensibility. The stress–optical behavior in this temperature range is characterized as Regime I–II–III behavior with an initial glassy component.

Stretching the material at temperatures near the T_g (below $T_g + 14$ °C) (130 °C) glassy behavior exists in the initial deformation stage. This becomes more pronounced and the stresses corresponding to the glassy component increase as the temperature decreases. As the deformation proceeds the material exhibits rubber-like deformation following 'Regime I', the slope of which decreases with increasing temperature. Following this regime I behavior the birefringence starts to reach a plateau with significant stress increase exhibiting Regime III behavior. The material in this temperature range

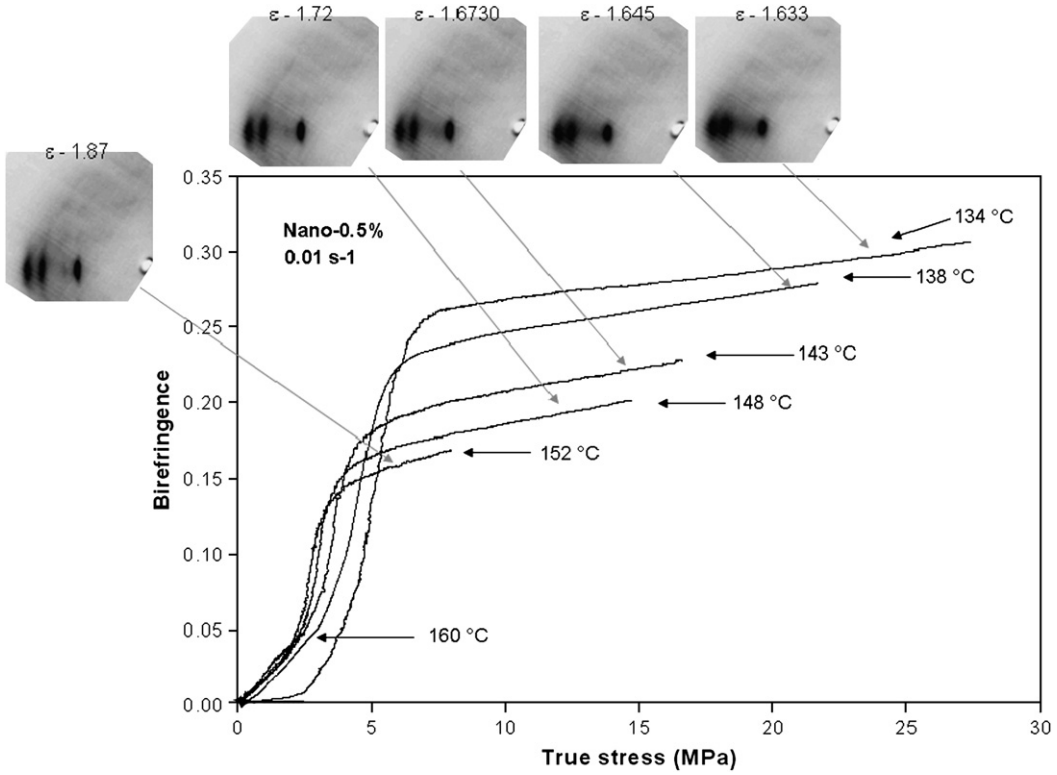

Fig. 13. Temperature effect on the stress–optical behavior of PEN with 0.5 wt% nanoparticles stretched at 0.01 s^{-1} engineering strain rate and final stretch ratio 4×.

does not exhibit regime II behavior which is normally associated with crystallization. Stress–optical behavior close to T_g is then characterized by a Regime I–III behavior with an additional glassy component and the absence of Regime II. These are illustrated in the inset of Fig. 11 where all idealized regimes together with glassy regime are indicated.

At higher stretching temperatures above $T_g + 32$ °C, relaxation clearly dominates the stress–optical behavior as shown by the broad equatorial peaks in the WAXD pattern. The initial glassy component is completely absent and the stress–optical behavior remains in the linear Regime I and does not exhibit Regimes II and III in the stress–optical behavior as they are successively eliminated with higher stretching temperatures as chain relaxation becomes dominant. WAXD patterns show that stretching at low temperatures leads to a highly oriented structure with low three-dimensional order and high translational disorder. As the stretching temperature is increased the orientation decreases due to relaxation and at the same time a three-dimensional crystal structure is developed.

Plotting the slopes of the glassy component and Regime I for different temperatures above the T_g (Fig. 12) for all the three nanocomposites shows that beyond a critical temperature approximately $1.2 \times T_g$ (°C) and around $1.07 \times T_g$ (K) the glassy component disappears and the Regime I slope becomes equal to the stress–optical constant and is almost independent of temperature from thereon. This transformation in the material behavior confirms that there is some molecular transition taking place. It appears from the data that below a certain temperature $1.07 \times T_g$ (K) the material deformation behavior is characterized by an initial glassy behavior with low birefringence rise which converts into a rubbery deformation behavior with further stretching. However, stretching above this temperature $1.07 \times T_g$ (K) the initial glassy behavior is completely non-existent and the material follows the rubbery deformation from the start of the stretching process with Regime I following the stress–optical rule.

These observations point to the 'liquid–liquid transition temperature (T_{ll})' as described by Boyer and later on by Frenkel [22]. According to Boyer T_{ll} represented a temperature above which the entire polymer chain is free to move as a unit and below which the material has some structure and is represented as a 'hindered liquid' or a 'fixed liquid state'. Frenkel finally associated the concept of 'segmental melting' at T_{ll}, above which the entropy of the polymer chains gives the driving force to free itself from the segmental restraints. They have shown with experimental evidences the T_{ll}–T_g relationship as well as the frequency dependence of T_{ll} exhibiting that T_{ll} is not a thermodynamic transition but has a kinetic nature. Similar observations have been made by us, as shown in Fig. 14, the correlation between T_g and this transition temperature holds well for different nanoparticle concentrations. In other words as the T_g of PEN changes with the addition of nanoparticles, so does this transition temperature. Also this transition is shown to be a function of stretching rate (Fig. 15). Correlating these concepts with our observations, the material below a certain temperature is in a 'fixed liquid' state due to segmental–segmental correlations as the

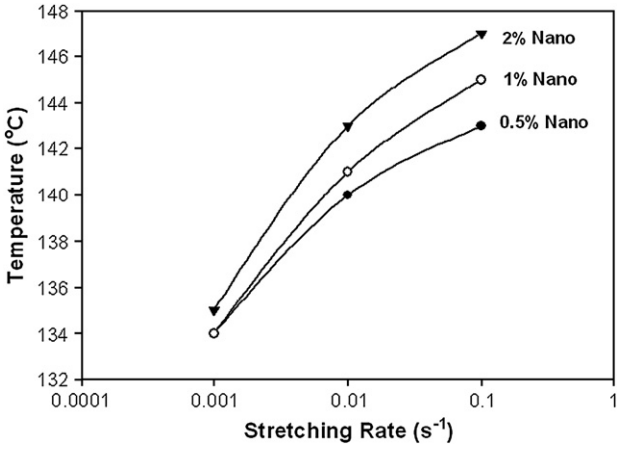

Fig. 15. T_{ll} as a function of engineering strain rate for different nanoparticle concentrations.

stretching behavior shows an initial glassy behavior. When stretched above T_{ll} 'segmental melting' occurs due to the increase in entropy of the system resulting in a rubbery deformation behavior which is devoid of the initial glassy component and Regime I follows the stress–optical rule.

Considering the stress–optical behavior at 138 °C which is about 2 °C below the T_{ll} transition (Fig. 16), the behavior is non-linear and it is very difficult to determine the end points of different regimes or, in other words, the transition from glassy behavior to the linear Regime I and further deviation to Regime II though present are very gradual. At 148 °C which is about 8 °C above T_{ll}, the transitions from one regime to another become very clearly defined. At and above the latter temperature, the initial slope of the curves becomes independent of temperature (see regime I marked by dashed line).

The birefringence–true strain behavior of 2% and 0.5% nanocomposite is shown in Figs. 17 and 18. The strain–optical behavior for 0.5% nanocomposite shows that at low temperatures (below 138 °C) the birefringence change with true strain is quite linear after the initial non-linear transient. However, increasing the stretching temperature beyond T_{ll} (above 143 °C) the change in birefringence becomes quite non-linear with a clear upturn at intermediate true strain values signifying

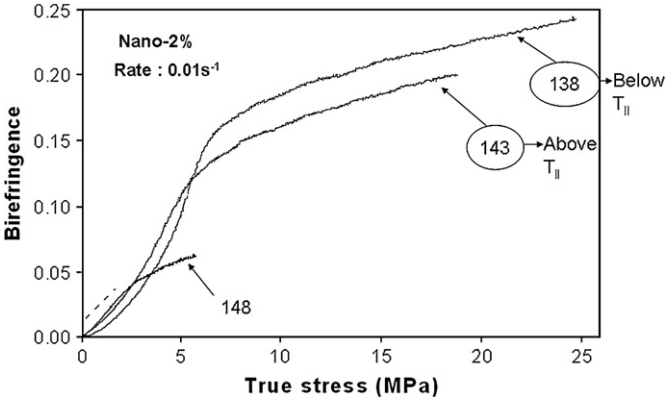

Fig. 16. Disappearance of non-linearity above T_{ll} for PEN with 2 wt% nanoparticles stretched at 0.01 s^{-1} engineering strain rate and final stretch ratio 4×.

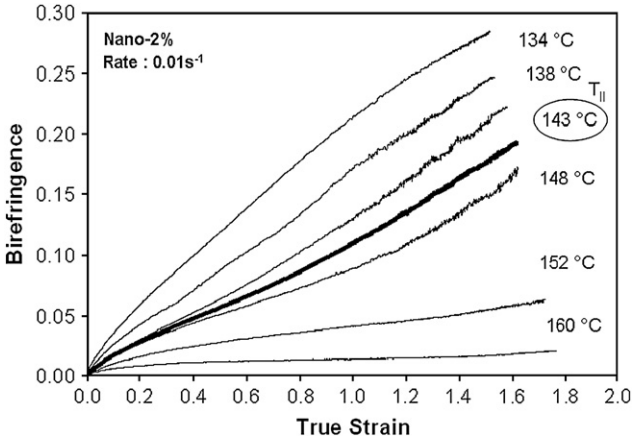

Fig. 17. Temperature effect on the strain–optical behavior of PEN with 2 wt% nanoparticles stretched at 0.01 s^{-1} engineering strain rate and final stretch ratio 4×.

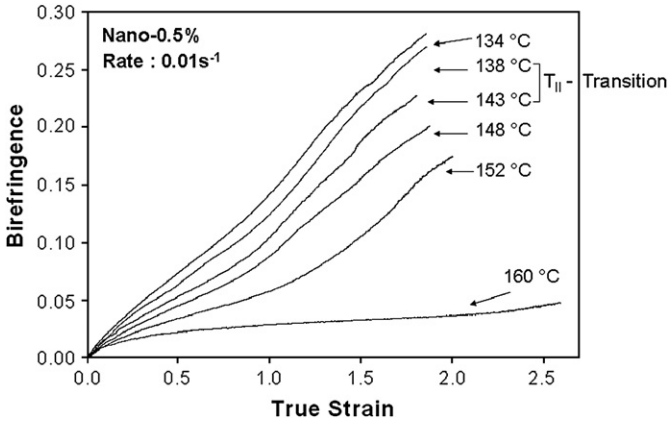

Fig. 18. Temperature effect on the strain–optical behavior of PEN with 0.5 wt% nanoparticles stretched at 0.01 s^{-1} engineering strain rate and final stretch ratio 4×.

spontaneous deformation processes occurring in the material. Finally with increasing the temperature to 160 °C the birefringence remains essentially constant as the orientation relaxation becomes dominant at these temperatures.

Increasing the nanoparticle concentration to 2 wt%, it is observed that the T_{II} transition though occurring does not have a clear effect on the birefringence–true strain behavior. This is because the necking mechanism that is prevalent in 0.5 wt% nanocomposite is eliminated at 2 wt% nanoparticle concentration and crystallinity is also decreased.

3.6. Effect of nanoparticles on the mechano-optical behavior

3.6.1. Stress–optical behavior

The stress–optical behavior of the nanocomposites as a function of nanoparticle content is shown in Fig. 19. All the nanocomposites are stretched at $T_g + 20$ °C for each composition at a stretching rate of 0.001 s^{-1}. The slope of Regime I remains almost the same with increasing the nanoparticle

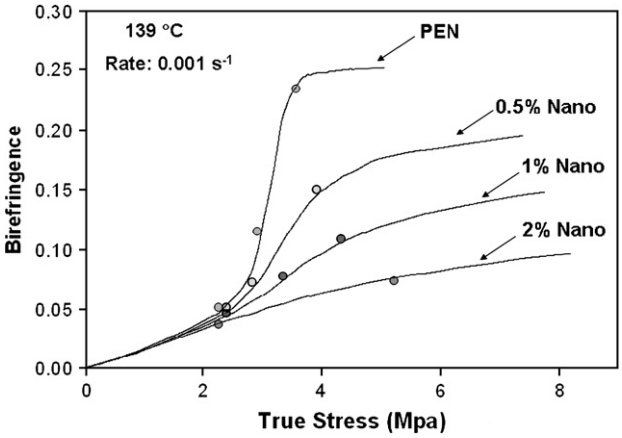

Fig. 19. Effect of nanoparticle concentration on the stress–optical behavior at 0.001 s^{-1} engineering strain rate and stretch ratio 4×.

content in the material. The Regime II slope, on the other hand, decreases with the addition of nanoparticles.

In parallel with the stress–optical behavior, Fig. 20 illustrates that the increase in crystallinity observed with deformation becomes quite rapid beyond a critical true strain of about 1.2 for neat PEN. However, the addition of nanoparticles decreases the slope of this region indicating that the development of crystallinity is adversely affected by the addition of nanoparticles.

The transition from Regime II to Regime III also becomes much smoother with increasing nanoparticle concentration in stress–optical behavior. The reason for this behavior is also the decline in increasing crystallinity. As the crystallinity in the material decreases, the physical network of crystallites formed in the material at the end of Regime II does not lock-in the structure. This, in turn, results in incomplete arrest of deformation resulting in a slow continuation of the orientation process with deformation manifested in slow birefringence increase. Comparing this with stress–optical behavior of PEN, the transitions are much sharper in PEN due to comparatively higher crystallinity which locks in the structure arresting the deformation, so there is no increase in the birefringence in Regime III.

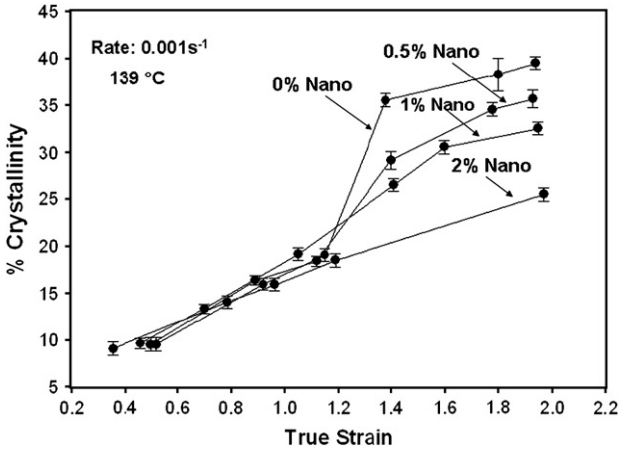

Fig. 20. Change in % crystallinity as a function of true strain.

3.6.2. Strain–optical behavior

Strain–optical behavior as influenced by the nanoparticles is shown in Fig. 21. The birefringence–true strain plots clearly show that the final true strain in the material decreases with increasing the nanoparticle concentration for the same macroscopic stretch ratio applied. This indicates that as the nanoparticle concentration is increased, the material is becoming stiffer. Hence the stress in the center portion of the sample, where all our measurements refer to, increases as it reaches its strain hardening earlier leading to arrest of deformation at lower strains and thus allowing other portions of the sample to deform. This results in production of uniform films along the stretching direction.

3.6.3. Strain rate behavior

The true (local) strain rate is calculated from the temporal variation of true strain. Influence of nanoparticles on the latter is shown in Fig. 22 for samples all stretched at 0.001 s^{-1} (macro)stretching rate. Even though the machine-applied macrostretching rate is constant, the true strain rate at the midsection of the sample is not. At early stages of deformation, the strain rate is around 0.001 s^{-1} nearly following what is expected in materials deforming affinely. Following this early stage, the strain rate sharply rises in the case of PEN indicating spontaneous deformation at the midsection of the sample where all the measurements are made. With the addition of nanoparticles the peak in strain rate diminishes and finally is entirely suppressed at 2% nanoparticle concentration. With further stretching, the strain rate rapidly decreases ultimately reaching almost zero value at the midsection of the sample for PEN and consistently higher non-zero values with the addition of nanoparticles.

3.7. Structural studies

The structural evolution as well as the ordering mechanisms responsible for the Regimes (Fig. 11, inset) observed in real time mechano-optical behavior is investigated using off-line characterization performed at different transition zones in the stress–optical behavior. The samples are rapidly cooled below the glass transition temperature after being stretched to a series of deformation levels. This was done to suppress significant relaxation effects during sample removal from the machine. In this process, some relaxation can be induced in the material which could have an influence on the final structure. However, the trends in the structural evolution processes can be exhibited through such experimentation. The results of off-line X-ray, DSC crystallinity, orientation and crystal size analysis together with the stress–optical behavior for films stretched at $T_g + 20$ °C are presented in Figs. 23–25. The material stretched under these conditions is above the temperatures where the initial glassy behavior is present (e.g. above the T_{ll} transition). As indicated earlier, the films exhibit three different stress–optical regimes (Fig. 11). Until the end of regime I, X-ray patterns and DSC crystallinity measurements show that the structure of films remains essentially in the amorphous state with crystallinity levels remaining well below 10%. With further deformation, deviation into Regime II of the stress–optical behavior is observed with the development of very sharp equatorial (010) peak. This indicates the presence of very highly oriented chains exhibiting substantial axial translational disorder as evidenced by the concurrent absence of off-equatorial peaks and higher order peaks. Such a WAXD pattern is a clear indication of ‘‘nematic-like’’ order. In this type of order, significant chain translational disorder along the stretching direction leads to absence of off-equatorial peaks. We believe that these ordered regions are created at the nodes of the entanglement network where the polymer chains are highly stretched and they further act as junction points of the long range network which once formed cause rapid increase of birefringence. These regions also act as a precursor to the strain induced crystallization process which progresses with further deformation. A steep rise in strain rate (Fig. 22) occurs a little before the materials' structure transitions from amorphous to the nematic order and steep birefringence rise starts to appear that indicates that after a certain level of deformation long range ‘‘connected’’ network of

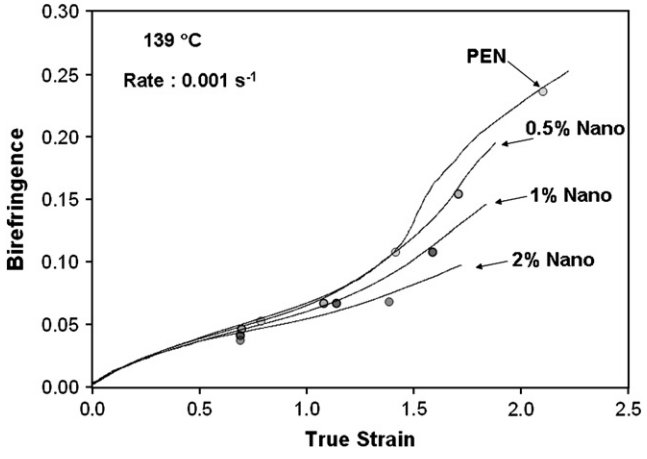

Fig. 21. Effect of nanoparticle on the strain–optical behavior stretched at 0.001 s^{-1} engineering strain rate and stretch ratio 4×.

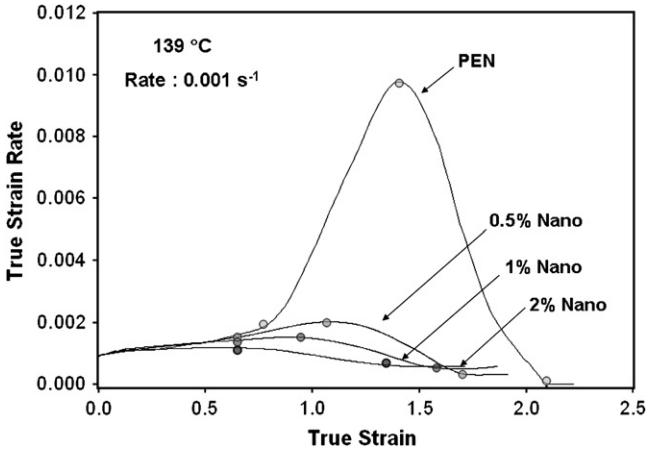

Fig. 22. Effect of nanoparticle concentration on the true strain rate behavior stretched at 0.001 s^{-1} macroscopic engineering strain rate.

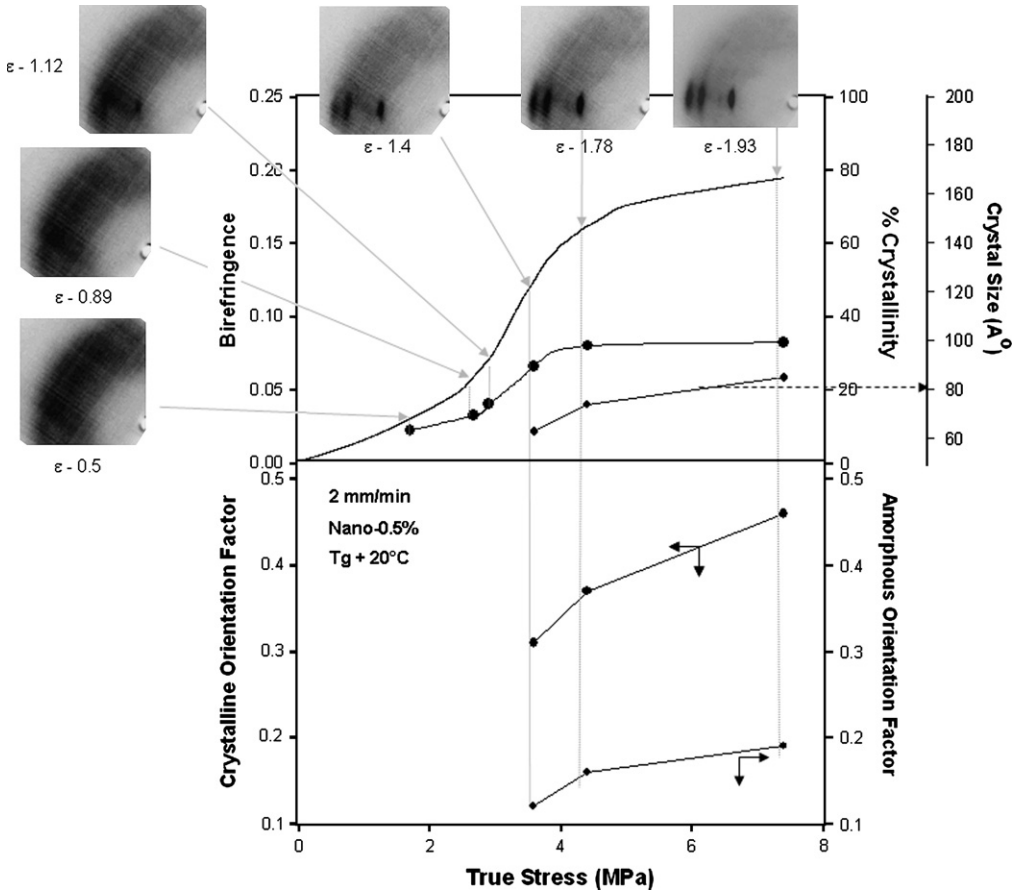

Fig. 23. Stress–optical behavior of PEN with 0.5 wt% nanoparticles stretched at $T_g + 20\,^{\circ}C$ and final stretch ratio 4× with corresponding WAXD patterns, % crystallinity and orientation analysis.

chains is formed as the 'coil-to-stretch' transition occurs facilitating efficient transmission of the stretching forces throughout the material causing the steep rise in strain rate as well as birefringence. Further stretching leads to the appearance of higher order peaks in the X-ray pattern and the off-equatorial peaks appear at high strains specifically in PEN–Nano-0.5% material suggesting development of a regular three-dimensionally ordered crystal structure in the material. Amount of crystallinity increases with stretching and so does the crystallite size as more chains get oriented with the progression of the stretching.

3.8. Effect of nanoparticle concentration

Beyond true strain of about 1.2, the crystallinity increase slows down with deformation with the addition of as little as 0.5 wt% nanoparticles (Fig. 20). With the addition of 2 wt% nanoparticles necking disappears and the crystallinity increase slows down substantially in parallel with the slow rise in birefringence with deformation. This drop in crystallinity and the subsequent slow rise in birefringence are explained by the decrease in orientation relaxation in the presence of nanoparticles that reduces the crystallizability of the oriented polymer chains by preventing them to become parallel and crystallize. It should be pointed out that at these very low temperatures, the chain diffusion is not expected to play a significant role. The primary mechanism that controls the crystallization is the preferential orientation and the resulting changes in configurational entropy. However, in order to crystallize, the oriented polymer chains must become parallel to each other. If they are oriented and remained locked-in in unfavorable orientations relative to each other, they certainly would not crystallize. The decrease in mobility of the polymer chains in the presence of hard clay surfaces decreases their relaxation substantially to become parallel to each other leading to substantial decrease in their strain crystallizabilities. The decrease in crystallization growth also results in the formation of a weaker long range load bearing network as there is lesser production of crystallites that form the nodes of the network. As a result of malformed crystalline network, orientation levels observed in amorphous regions become lower (Fig. 26). This combined effect of diminished crystallinity as well as lower amorphous orientation explains the decrease in birefringence as the nanoparticle concentration is increased in PEN.

However, the crystalline orientation factor increases with the addition of nanoparticles. This is contrary to the effect nanoparticles have on the bulk amorphous orientation (Fig. 26). This shows that the nanoparticles promote the alignment of polymer crystallites even though the amorphous

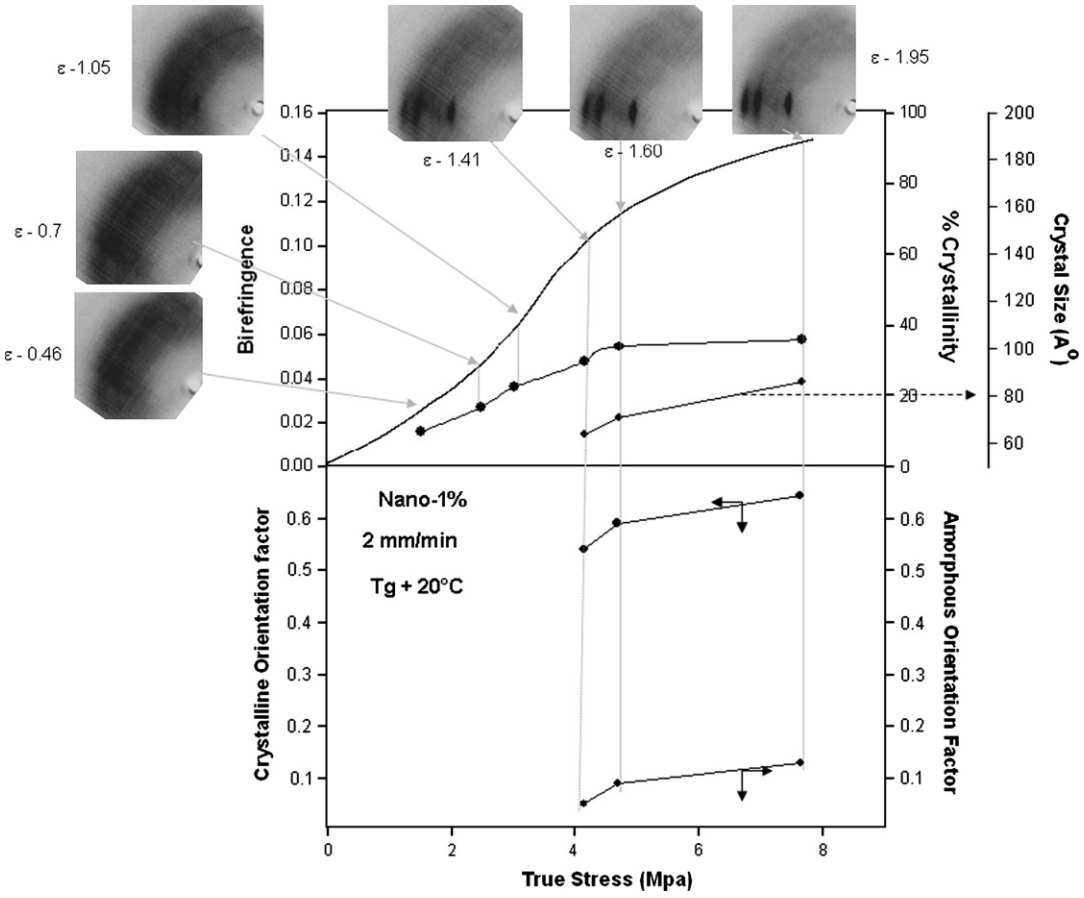

Fig. 24. Stress–optical behavior of PEN with 1 wt% nanoparticles stretched at $T_g + 20$ °C and final stretch ratio 4× with corresponding WAXD patterns, % crystallinity and orientation analysis.

orientation decreases with the addition of nanoparticles. Nanoparticles have been shown to act as nucleation agent as the increase in orientation in the presence of these particles decreases the cold crystallization temperature T_{cc}. We suspect that the crystallites develop in the vicinity of the nanoplatelets and the relaxation of polymer chains is suppressed in the proximity of the nanoparticles leading to sufficient levels of orientation which leads to oriented crystallization.

Summing up the effect of nanoparticles on the structure development of PEN nanocomposites it appears that the amount of crystallinity as well amorphous orientation decreases but the crystalline orientation increases with the addition of nanoparticles.

The influence of deformation on the cold crystallization temperature (T_{cc}) is plotted as a function of true strain for different nanoparticle contents as shown in Fig. 27 to see the trends in the material behavior as it indirectly indicates the orientation in the material. It is observed that initially the T_{cc} drops at a very steep rate in pure PEN as well as in the nanocomposites. However, around a true strain of 1 the slope of the T_{cc} drop slows down with the addition of nanoparticles resulting in a higher T_{cc} for the same true strain. This point also coincides with the start of orientation-induced crystallization in the material and indirectly agrees with the above observation that amorphous regions possess less orientation with the increase in clay nanoparticle.

3.9. Identification of phases

3.9.1. Nematic–crystalline transition

As shown in Fig. 28 for PEN–Nano-1% material, the mechano-optical behavior for the material stretched at 130 °C shows a significant initial glassy behavior followed by a steep rise in birefringence and finally the birefringence saturates with significant stress increase. The WAXD pattern collected on the sample at the end of the stretching process shows only the presence of a (010) equatorial peak. The remaining higher order peaks are absent with some diffuse scattering intensity in this area. Increasing the stretching temperature to 134 °C and higher leads to the appearance of higher order peaks namely $(\bar{1}10)$and (100) which become more distinct with higher stretching temperature. Concurrently, we see that the mechano-optical behavior also changes with the slope of Regime I decreasing progressively with increasing the temperature and the appearance of Regime II at 134 °C which is nonexistent at 130 °C. This positive deviation into Regime II and the appearance of clear higher order peaks are considered

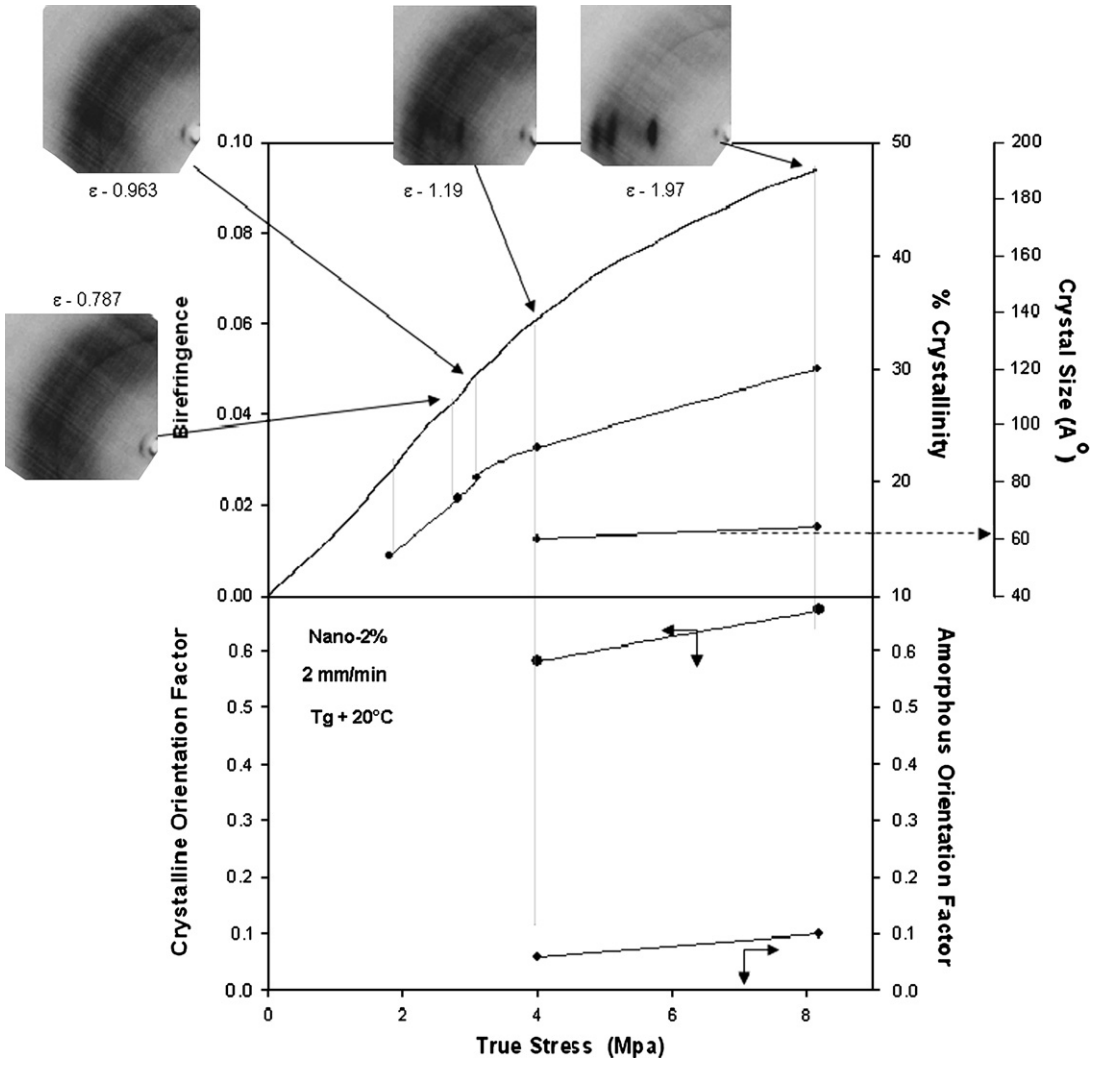

Fig. 25. Stress–optical behavior of PEN with 2 wt% nanoparticles stretched at $T_g + 20\,^{\circ}C$ and final stretch ratio 4× with corresponding WAXD patterns, % crystallinity and orientation analysis.

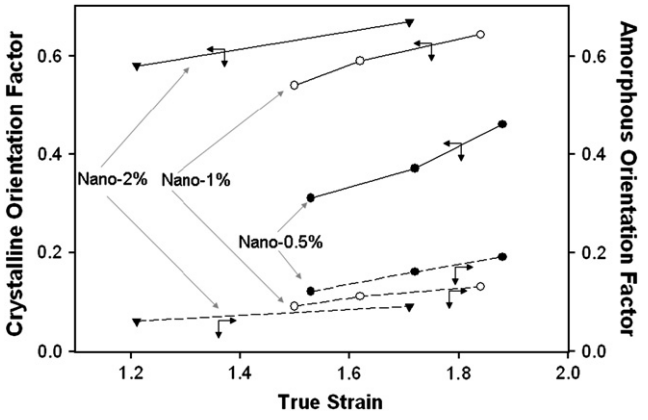

Fig. 26. Crystalline and amorphous orientation factors as functions of true strain.

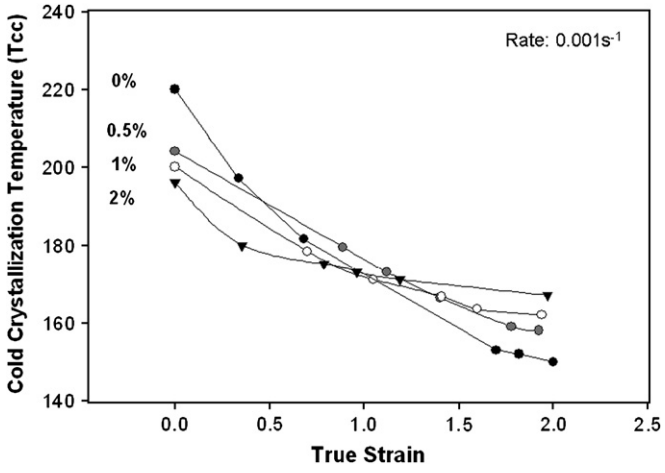

Fig. 27. Cold crystallization temperature as a function of true strain for different nanoparticle concentrations.

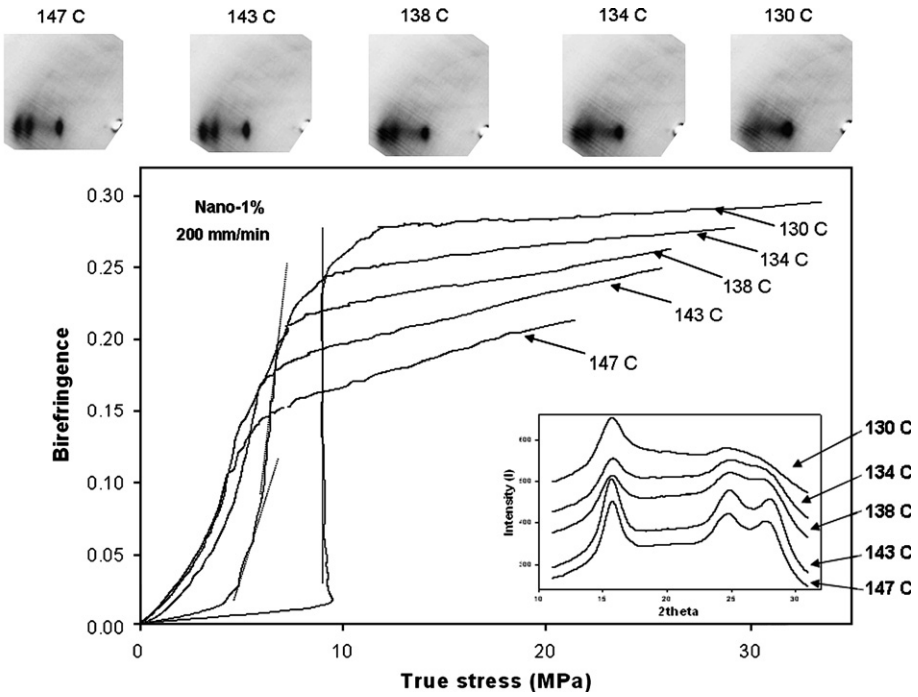

Fig. 28. Stress–optical behavior of PEN with 1 wt% nanoparticle at 0.1 s^{-1} and final stretch ratio 4× with corresponding WAXD patterns indicating nematic to crystalline transition.

as the transition point from nematic to strain induced crystallization.

3.9.2. Glassy to fluid transition (sometimes called T_{ll} transition)

This occurs at around $1.2 \times T_g$ (°C) or $1.07 \times T_g$ (K) as described earlier. Fig. 29 shows the deformation behavior of PEN–Nano-1% stretched at the rate of 0.01 s^{-1} at different stretching temperatures. The mechano-optical behavior at 135 °C shows an initial glassy portion. The slope of this glassy portion increases and the stresses related to this glassy region decrease with increasing temperature. Increasing the temperature by 2 °C to 141 °C completely eliminates this glassy behavior and the stress–optical behavior begins with Regime I following the stress–optical rule. This transition point is marked as transition temperature at which the initial glassy component in the stress–optical behavior completely disappears and Regime I follows the stress–optical rule.

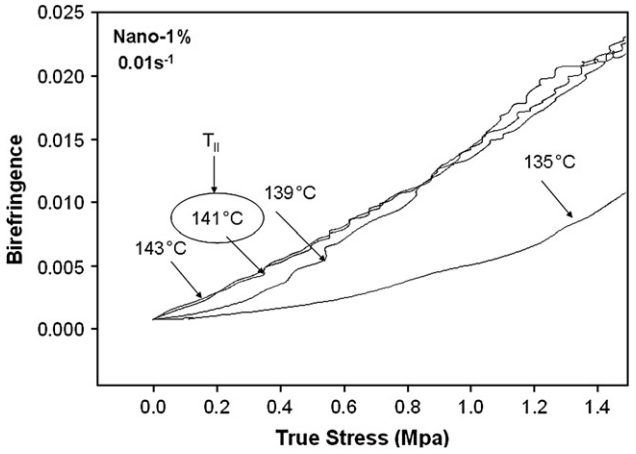

Fig. 29. Stress–optical behavior of PEN with 1 wt% nanoparticle at 0.01 s^{-1} and final stretch ratio 4× indicating liquid–liquid transition.

3.10. Dynamic phase diagram

According to the criteria defined above we determined the dynamic phase diagrams for the PEN nanocomposites with 0.5 wt%, 1 wt% and 2 wt% nanoparticle concentrations as shown in Figs. 30 and 31, respectively, only for 0.5 wt% and 2 wt% compositions. We are not showing 1% composition for brevity. Two critical transitions were observed.

(1) Nematic–crystalline transition;
(2) Glassy to liquid (T_{ll}) transition.

In our previous paper [23] on PEN–PEI blends we were able to observe a crystalline to amorphous transition in the material. However, we believe that the local orientation amplification effect induced by the nanoparticles prevents the material from going into a completely amorphous state at high stretching temperatures even though relaxation is dominant.

The T_{ll} transition as shown in Figs. 14 and 15 is a function of nanoparticle concentration as well as stretching rate so it certainly is not a thermodynamic property of the material and more a kinetic property of the material. The change in the T_{ll} transition with stretching rate is also investigated and shown in Fig. 15. For 2% nanocomposition at very low

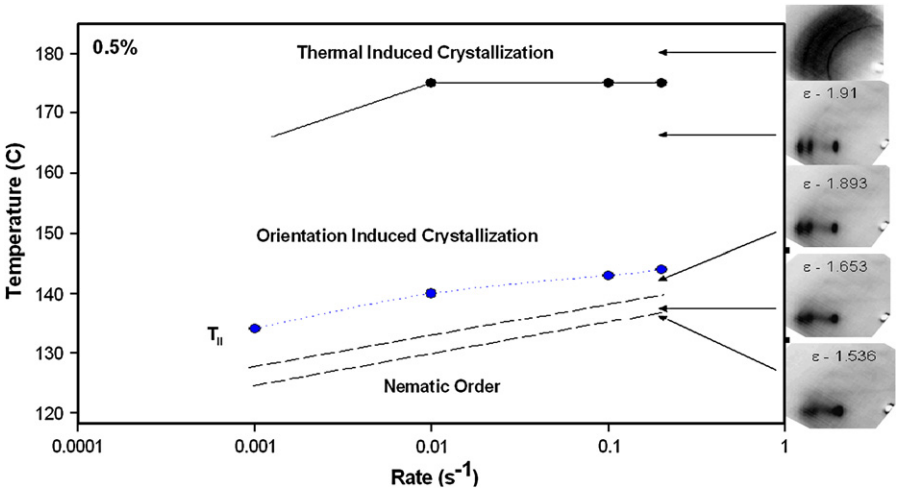

Fig. 30. Dynamic phase diagram for PEN with 0.5 wt% nanoparticle concentration.

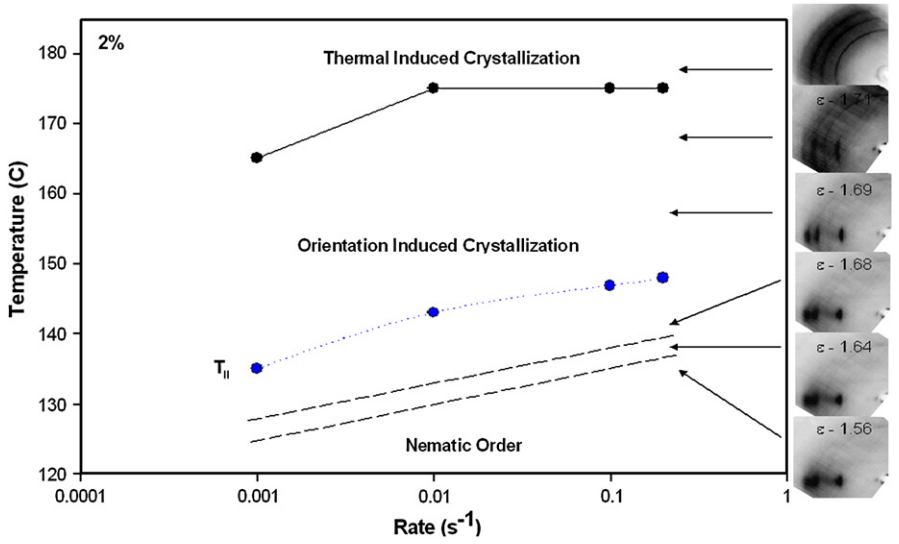

Fig. 31. Dynamic phase diagram for PEN with 2 wt% nanoparticle concentration.

stretching rate of 0.001 s^{-1} the transition occurs at 135 °C. As the stretching rate is increased the transition occurs consistently at higher temperatures finally at 147 °C for the highest stretching rate of 0.1 s^{-1}.

Finally increasing the temperature above 178 °C for about 20 min preheating time results in thermally induced crystallization as the nucleation and chain diffusion rates begin to become significant. This marks the point above which the material thermally crystallizes. This transition point is shown as a function of stretching rate in the dynamic phase diagram occurring at lower temperatures for lower rates as the sample is exposed to these temperatures longer during deformation and as a result thermally activated crystallization becomes appreciable at lower temperatures due to this prolonged thermal exposure of the sample to processing temperatures at these lower rates. It should be pointed out that the increase of clay concentration broadens the gap between the nematic transition and T_{II} at all stretching rates as these samples exhibit wider temperature range where the glassy behavior remains effective.

4. Conclusions

PEN nanocomposites exhibit a three-regime non-linear stress–optical behavior along with an additional glassy component. Nanoparticles do not have significant contribution to the birefringence development of PEN before strain induced crystallization. After crystallization is induced, the birefringence increase is greatly subdued with the addition of nanoparticles due to lower crystallinity and amorphous orientation. A kinetic transition (T_{II}) is observed below which the stress–optical behavior includes an initial glassy component attributed to stiff segmental correlations. At low stretching temperatures, the films remain in a 'nematic-like' state that converts into orientation-induced crystallization at intermediate temperatures. Finally, stretching at high enough

temperatures, where the relaxation process dominates the material deformation behavior, PEN nanocomposites still crystallize indicating that nanoparticles promote local chain orientation not allowing complete relaxation of the chains adjacent to them or entrapped in the narrow passages between the particles and/or intergallery spacings. Based on these quantitative results "dynamic phase diagrams" were constructed for nanoparticle filled polyethylene naphthalate.

References

[1] Toki S, Valladares D, Sen TZ, Cakmak M. ANTEC Proc 2001:1830.
[2] Koike Y, Cakmak M. Polymer 2003;44:4249.
[3] Lee SW, Cakmak M. J Macromol Sci Phys 1998;B37(4):501–26.
[4] Kim JC, Cakmak M. J Appl Polym Sci 1997;65:2059.
[5] Usuki A, Kojima Y, Kawasumi M, Okada A, Fukushima Y, Kurauchi T, et al. J Mater Res 1993;8:1179–83.
[6] Vaia RA, Kramer EJ, Giannelis EP. Macromolecules 1995;28:8080–5.
[7] Blumstein A. J Polym Sci 1965;A3:2665–73.
[8] Burnside SD, Giannelis EP. Chem Mater 1995:1597–600.
[9] Giannelis EP, Krishnamoorti R, Manias E. Adv Polym Sci 1999;118: 108–47.
[10] Koike Y, Cakmak M. Macromolecules 2004;37:2171–81.
[11] Valladares D, Toki S, Sen TZ, Yalcin B, Cakmak M. Macromol Symp 2002;185:149–66.
[12] Ryu DS, Inoue T, Osaki K. Polymer 1998;39:2515–20.
[13] Martins CI, Cakmak M. Macromolecules 2005;38(10):4260–73.
[14] Kroger M, Luap C, Muller R. Macromolecules 1997;30:526–39.
[15] Ouchi IH, Aoki S, Shimotsuma T, Asai M. Proceedings of the 17th congress on materials research, Japan; March 1974. p. 217.
[16] Mencik Z. Chem Prum 1967;17:78.
[17] Cheng SZD, Wunderlich W. Macromolecules 1988;21:789.
[18] Lee SW, Cakmak M. Polymer 1995;36:4039–54.
[19] Yalcin B, Cakmak M. Polymer 2004;45:6623–38.
[20] Cakmak M, Kim JC. J Appl Polym Sci 1997;61:739.
[21] Hardy L, Stevenson I, Boiteux G, Seytre G, Schönhals A. Polymer 2001; 42:5679.
[22] Boyer RB. Polymer yearbook; 1998. p. 234–337;
And also see: In: Keinath Steven E, Miller Robert L, Rieke James K, editors. Order in the amorphous "state" of polymers. New York: Plenum Press; 1987.
[23] Kanuga K, Cakmak M. Macromolecules 2005;38(23):9698–710.